Hindawi Publishing Corporation
Journal of Applied Mathematics
Volume 2015, Article ID 374325, 10 pages
http://dx.doi.org/10.1155/2015/374325

*Research Article*

# An UWB LNA Design with PSO Using Support Vector Microstrip Line Model

**Salih Demirel, Filiz Gunes, and A. Kenan Keskin**

*Electronics & Communication Engineering Department of Yildiz Technical University, Esenler, 34220 Istanbul, Turkey*

Correspondence should be addressed to A. Kenan Keskin; kkeskin@yildiz.edu.tr

Received 13 March 2015; Accepted 2 August 2015

Academic Editor: Wei Fang



A rigorous and novel design procedure is constituted for an ultra-wideband (UWB) low noise amplifier (LNA) by exploiting the 3D electromagnetic simulator based support vector regression machine (SVRM) microstrip line model. First of all, in order to design input and output matching circuits (IMC-OMC), source $Z_S$ and load $Z_L$ termination impedance of matching circuit, which are necessary to obtain required input VSWR ($V_{i\text{req}}$), noise ($F_{\text{req}}$), and gain ($G_{T\text{req}}$), are determined using performance characterisation of employed transistor, NE3512S02, between 3 and 8 GHz frequencies. After the determination of the termination impedance, to provide this impedance with IMC and OMC, dimensions of microstrip lines are obtained with simple, derivative-free, easily implemented algorithm Particle Swarm Optimization (PSO). In the optimization of matching circuits, highly accurate and fast SVRM model of microstrip line is used instead of analytical formulations. ADCH-80a is used to provide ultra-wideband RF choking in DC bias. During the design process, it is aimed that $V_{i\text{req}} = 1.85$, $F_{\text{req}} = F_{\min}$, and $G_{T\text{req}} = G_{T\max}$ all over operating frequency band. Measurements taken from the realized LNA demonstrate the success of this approximation over the band.

## 1. Introduction

Nowadays, RF circuits have many important usage areas in communication systems. In front-end systems, low noise amplifiers are used in first stage of receiver parts because of their low signal to noise ratio which provides possibility of getting more incoming signal from ambient. Besides, ultra-wideband structures are usually demanded because of their multiple operation frequency choices. To design such ultra-wideband low noise amplifiers, a fast, highly accurate, and feasible method which combines many areas like circuit theory, microwave, and so forth is required [1–4].

Microstrip transmission lines are popularly used to design microwave circuits because of low cost, flexible structure, and easy production. In order to design microstrip matching network of amplifier, a highly accurate, efficient, and fast microstrip transmission line model is required. After obtaining such a model, the lines are synthesized with circuit theory to compose matching circuit. High frequency elements of RF circuit could be analyzed and optimized with numerical programs, but these numerical methods could be slow because of their solution methodology. This problem would be solved using knowledge based model of RF elements. Learning machine models like artificial neural network (ANN), general regression neural network (GRNN), support vector regression machines (SVRM), and so forth are frequently used in many areas. Microwave applications of learning machines have been issued in previous works such as microwave transistor modeling with ANN [5, 6], SVRM model of a transmission line [7]. Obtained models of different RF elements could be used to synthesise RF circuits.

A low noise microwave amplifier is composed of input and output matching circuit (IMC and OMC), microwave transistor, and DC bias. In order to design IMC and OMC, input and output impedance ($Z_S, Z_L$) of matching circuits are required for requested transducer gain ($G_T$), input VSWR ($V_i$), and noise figure ($F_i$) of low noise amplifier. This impedance is acquired from performance characterisation of employed microwave transistor [8, 9]. After that, dimensions of microstrip lines in matching circuits are obtained with an optimization algorithm. In the literature, different kinds of optimization algorithms, such as genetic, particle swarm, have been successfully utilized together in microwave circuit and antenna design [10–13].

In this paper, an ultra-wideband low noise microstrip amplifier is designed with novel methodology and then fabricated and measured. Firstly, highly accurate and fast SVRM model of microstrip line is created. Secondly, input and output impedance of matching networks are obtained with performance characterisation of NE3512S02 high technology transistor all over the operation band for requested $G_{T\text{req}}$, $V_{i\text{req}}$, and $F_{\text{req}}$. After that, microstrip line dimensions of IMC and OMC are optimized using evolutionary global optimum searcher PSO [14, 15]. In optimization process, microstrip lines are represented by SWRM model. Finally, designed amplifier is fabricated and measured, and then results are compared with each other.

## 2. Performance Characterisation for a Microwave Transistor

*2.1. Compatible $(F, V_i, G_T)$ Triplets and the $(Z_S, Z_L)$ Terminations.* In a typical design problem of a basic microwave amplifier employing per se a FET as an active device, the active device can be represented by a two-port circuit. Since in such a system all the main performance components of $F$, $V_i$, and $G_T$ are determined by the active device employed, the device must be identified by all its compatible ($F$, $V_i$, and $G_T$) performance triplets and their ($Z_S = Z_{\text{out}}\{\text{IMC}\}$, $Z_L = Z_{\text{in}}\{\text{IMC}\}$) terminations (Figure 1). Here the $(Z_S, Z_L)$ terminations are the simultaneous solutions of the following nonlinear performance equations of the transistor subject to the physical realization conditions:

$$F = \frac{(S/N)_i}{(S/N)_O} = F\{R_S, X_S\} = F_{\min} + \frac{R_N}{|Z_{\text{opt}}|^2}\frac{|Z_S - Z_{\text{opt}}|^2}{R_S}. \quad (1)$$

$$V_i = V_i\{R_S, X_S, R_L, X_L\} = \frac{1+|\rho_i|}{1-|\rho_i|}, \quad \rho_i = \frac{Z_S - Z_{\text{in}}^*}{Z_S + Z_{\text{in}}}. \quad (2)$$

$$G_T \triangleq \frac{P_L}{P_{AVS}} = G\{R_S, X_S, R_L, X_L\} = \frac{4R_S R_L |z_{21}|^2}{|(z_{11}+Z_S)(z_{22}+Z_L) - z_{12}z_{21}|^2}. \quad (3)$$

Here the physical realization conditions can be expressed as follows:

$$\text{Re}\{Z_{\text{in}}\} = \text{Re}\left\{z_{11} - \frac{z_{12}z_{21}}{z_{22}+Z_L}\right\} > 0. \quad (4)$$

$$\text{Re}\{Z_{\text{out}}\} = \text{Re}\left\{z_{22} - \frac{z_{12}z_{21}}{z_{11}+Z_S}\right\} > 0. \quad (5)$$

$$F \geq F_{\min}, \quad V_i \geq 1, \quad G_{T\min} < G_T \leq G_{T\max}, \quad (6)$$

where $z_{ij} = r_{ij} + jx_{ij}$, $i, j = 1, 2$, are the open-circuited parameters of the transistor and the conditions given by (4) and (5) ensure the stable operation of the active device.

The simultaneous solution $(Z_S, Z_L)$ sets of the nonlinear performance equations (1), (2), and (3) subject to the physical realization conditions given by (4), (5), and (6) are obtained in the three main steps which are determinations of (i) the Possible Solution Region (PSR); (ii) the Unconditionally Stable Working Area (USWA); (iii) Variations of the Constrained Gain in the USWA. Finally, the Possible Solution Region (PSR) and the Unconditionally Stable Working Area (USWA) are gathered together with the Variations of the Constrained Gain in the input impedance $Z_{\text{in}}$ plane and the resulted configuration may be called "design configuration" which is dependent on the device operation parameters of the frequency $f$, bias condition IDS, VDS.

*2.2. The Possible Solution Region (PSR).* Examination of the nonlinear performance equations (1), (2), and (3) reveals, respectively, the following variations for the noise figure $F$, input VSWR $V_i$, and gain $G_T$ in the $Z_S$ plane taking $Z_L$ as a control parameter:

(i) All the source $Z_S = R_S + jX_S$ terminations that satisfy $F\{R_S, X_S\} = F_{\text{req}} = \text{const.}$ in (1) take place on the circle in the $Z_S$ plane whose equation is

$$|Z_s - Z_{cn}| = r_n, \quad (7)$$

where $Z_{cn}$ and $r_n$ are the center and radius of the noise circle which can be, respectively, given by [8]

$$Z_{cn} = R_{\text{opt}} + N + jX_{\text{opt}}, \quad r_n = \sqrt{N(N+1) + 2R_{\text{opt}}}, \quad (8)$$

where $Z_{\text{opt}} = R_{\text{opt}} + jX_{\text{opt}}$ is the source termination providing the minimum noise figure to the transistor and the real constant $N$ is described in terms of the noise parameters such that

$$N \triangleq \frac{(F_{\text{req}} - F_{\min})}{2R_n}|Z_{\text{opt}}|^2. \quad (9)$$

Here when $F_{\text{req}} = F_{\min}$, then $N = 0$, $r_n = 0$, and the noise circle becomes a point of the optimum noise impedance $Z_{\text{opt}}$. While $F_{\text{req}} > F_{\min}$, the centers shift to the right on the $X = X_{\text{opt}}$ line and the radii increase according to (8).

(ii) All the source $Z_S = R_S + jX_S$ terminations that satisfy $V_i = V_i\{R_S, X_S, R_L, X_L\} = V_{i\text{req}} = \text{const}$ for a fixed passive load $Z_L$ take place on the circle of

$$|Z_S - Z_{cv}| = r_v, \quad (10)$$

where $Z_{cv}$ is the center phasor and $r_v$ is the radius of

$$Z_{cv} = \frac{1+|\rho_{\text{in}}|^2}{1-|\rho_{\text{in}}|^2}(R_{\text{in}} - jX_{\text{in}}), \quad r_v = 2\frac{|\rho_{\text{in}}|}{1-|\rho_{\text{in}}|^2}R_{\text{in}}. \quad (11)$$

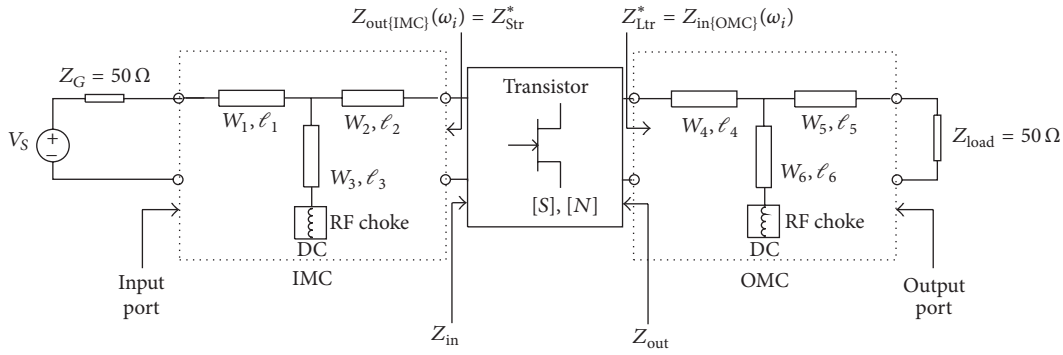


FIGURE 1: Low noise amplifier with $T$-type microstrip line matching networks.

A $V_i = V_{ireq}$ circle corresponds to a constant gain circle for a fixed load $Z_L$, which can be expressed using (2) and (3) as

$$G_T = \left(1 - |\rho_{in}|^2\right) \frac{R_L}{R_{in}} \frac{|z_{21}|^2}{|z_{22} + Z_L|^2}. \tag{12}$$

Therefore, only the required noise and the input VSWR circles are sufficient to be taken into account in the $Z_S$ plane. As already seen from (7), (8), and (9), while the required noise circle is fixed in the $Z_S$ plane, the required input VSWR circle can travel, depending on the load impedance $Z_L$, via the input impedance $Z_{in}$ in a manner given by the center and radius relations in equation given by (11). Thus, the following situations are possible to obtain using the load impedance $Z_L$ as the control parameter: these circles may not touch which corresponds to the no-solution case, they become tangential, or they cut each other [8]. In the following step, each of these positions is mapped into the $Z_{in}$ plane.

(iii) The equations of the $T_1$ and $T_2$ boundary circles between the solution and no-solution regions in the $Z_{in}$ plane can be obtained from mapping of the external and internal tangential positions of the VSWR circle with respect to the noise circle, respectively, from the $Z_S$ plane as follows:

$$|Z_{cn} - Z_{cv}|^2 = (r_n \pm r_v)^2. \tag{13}$$

Substituting $Z_{cn}$, $Z_{cv}$, $r_n$, and $r_v$ from (8), (9), and (11) into the (13), the center phasors $Z_{ct1}$, $Z_{ct2}$ and radii $r_{t1}$, $r_{t2}$ of the $T_1$ and $T_2$ circles can be obtained, respectively, as

$$Z_{ct1} = R_{cn}U + r_nV - jX_{opt}. \tag{14}$$

$$r_{t1} = \sqrt{|Z_{ct1}|^2 - |Z_{opt}|^2}. \tag{15}$$

$$\Longleftrightarrow T_1 \text{ circle} \Longleftrightarrow \text{Region 2}$$

$$Z_{ct2} = R_{cn}U - r_nV - jX_{opt}. \tag{16}$$

$$r_{t2} = \sqrt{|Z_{ct2}|^2 - |Z_{opt}|^2}. \tag{17}$$

$$\Longleftrightarrow T_2 \text{ circle} \Longleftrightarrow \text{Region 4},$$

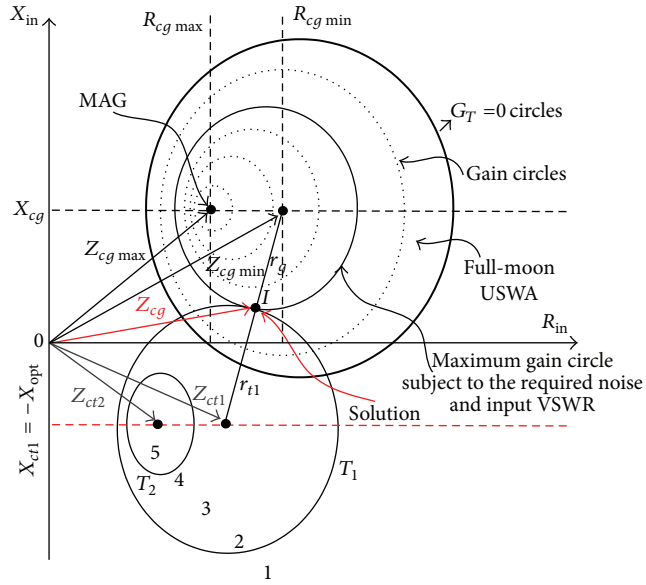


FIGURE 2: The full-moon USWA for the unconditional stability case is at the right hand side of the $Z_{in}$ plane.

where $U$ and $V$ stand for

$$U \triangleq \frac{1 + |\rho_{in}|^2}{1 - |\rho_{in}|^2},$$
$$V \triangleq \frac{|\rho_{in}|}{1 - |\rho_{in}|^2}. \tag{18}$$

As seen from (14) and (16), the centers of the $T_1$ and $T_2$ circles lie on the same imaginary axis, which is $X = -X_{opt}$, and it can also be proved using (14)–(17) that circle $T_2$ is always situated inside circle $T_1$ without touching as shown in Figure 2.

All the $Z_{in}$ values ensuring intersection positions of both the noise and input VSWR circles in the $Z_S$ plane are situated in Region 3 between the $T_1$ and $T_2$ circles in the $Z_{in}$ plane, which is shown in Figures 2 and 3. The remaining regions numbered 1 and 5, which are the outermost and innermost regions, respectively, are impossible solution regions that

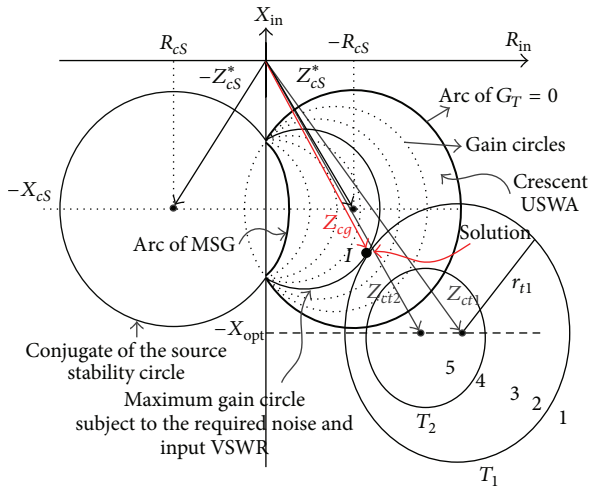


FIGURE 3: The crescent USWA for the conditional stability case takes place at left hand side of the $Z_{in}$ plane.

include $Z_{in}$ values controlling all the nontouching positions in the $Z_S$ plane (Figures 2 and 3).

In order to satisfy the physical realization conditions given by (4), (5), and (6), the Unconditionally Stable Working Area (USWA) and the gain circles constrained by the $V_{ireq}$ must also be constructed in the $Z_{in}$ plane; thus the design configuration will have been formed in the $Z_{in}$ plane.

*2.3. Design Configuration and Compatible Performance $(F, V_i, G_T)$ Triplets.* There are two types of the design configuration depending on the stability condition of the device:

(i) Design configuration for the absolutely stable device: the necessary and sufficient conditions for this case are as follows:

$$\begin{aligned} r_{11} &> 0, \\ r_{22} &> 0, \\ 2r_{11}r_{22} - r &> |z|, \\ z \triangleq z_{12}z_{21} &\triangleq r + jx. \end{aligned} \tag{19}$$

Examination of the gain equation given in (12) under the constraints of (19) reveals the nonintersection geometry of Figure 2, where the input stability circle is the $G_T = 0$ circle, since it is the geometric place of the mapped load impedance in the purely reactive nature $Z_L = jX_L$. Using (12), one may obtain the centers and radii of the gain circles taking place inside the $G_T = 0$ circle which are, respectively, as follows:

$$\begin{aligned} R_{cg} &= \frac{1}{2r_{22}}(Q - P), \\ X_{cg} &= \frac{1}{2r_{22}}(2x_{11}r_{22} - x), \end{aligned} \tag{20}$$

$$r_g = \frac{1}{r_{22}}\sqrt{P^2 - 2QP + |z|^2}, \tag{21}$$

$$\begin{aligned} P &\triangleq \frac{|z_{12}|^2}{1 - |\rho_i|^2}G_T, \\ Q &\triangleq 2r_{11}r_{22} - r. \end{aligned} \tag{22}$$

It can be seen from (20)–(22) that $R_{cg}$ decreases with the increase of $G_{Treq} \le G_{Tmax}$ when $X_{cg}$ remains constant (Figure 2) and the $G_{Tmax}$ is only achieved at the point where the $r_g$ equals zero. Setting $r_g$ to zero in (21) gives

$$\begin{aligned} G_{T\max} &= \left(Q - \sqrt{Q^2 - |z|^2}\right)\frac{1 - |\rho_i|^2}{|z_{12}|^2}. \\ Z_{i\max} &= Z_{cg\max} = R_{cg\max} + jX_{cg}. \\ R_{cg\max} &= \frac{1}{r_{22}}\left(Q^2 - |z|^2\right). \end{aligned} \tag{23}$$

The minimum gain limit circle is the $G_T = 0$ circle input stability circle whose center phasor $Z_{cg\min} = R_{cg\min} + jX_{cg\min}$ and $r_{g\min}$ can be given as follows:

$$\begin{aligned} R_{cg\min} &= \frac{Q}{2r_{22}}, \\ X_{cg\min} &= X_{cg}, \\ r_{g\min} &= \frac{|z|}{2r_{22}}. \end{aligned} \tag{24}$$

Because $Q$ is greater than $|z|$ for the absolutely stable device, $R_{cg\min}$ is greater than $r_{g\min}$, which results in a nonintersection geometry with the $G_T = 0$ circle being entirely in the right half of the $Z_{in}$ plane with the positive real part and enclosing all the circles for $G_T > 0$ (Figure 2). The region inside of the $G_T = 0$ circle is the Unconditionally Stable Working Area (USWA); since the device is unconditionally stable, all the compatible $(F, V_i, G_T)$ triplets take place in the intersection area between the PSR and USWA and any selection criteria to establish the design target space can be applied to them.

(ii) Design configuration for the conditionally stable device: in the case of the conditionally stable transistor, the USWA takes place between the input stability circle which is the $G_T = 0$ circle and the arc of the conjugate of the stability circle remaining in the right half of the $Z_{in}$ plane (Figure 3). The constrained gain formula equation (12) can be rearranged in terms of the radius and center of the source plane stability circle as

$$|Z_i|^2 + 2(R_{CS} + S)R_i + 2X_{CS}X_i + |Z_{CS}|^2 - {r_S}^2 = 0, \tag{25}$$

$$S \triangleq \frac{|z_{12}|^2 G_T}{2r_{22}\left(1 - |\rho_i|^2\right)}, \tag{26}$$

$$R_{CS} = -\frac{2r_{11}r_{22} - r}{2r_{22}},$$
$$X_{CS} = \frac{2x_{11}r_{22} - r}{2r_{22}}, \quad (27)$$
$$r_S = \frac{|z|}{2r_{22}}.$$

The features of the $G_T$ circles, which can be derived from (25)–(27), can briefly be expressed as follows (Figure 3):

(a) All $G_T$ circles cut the imaginary axis at the same points, which are the intersection points of the conjugate of the source plane stability circle with the same axis.

(b) The $G_T = 0$ circle whose center is $Z_{cg\min} = -R_{cs} - jX_{cs}$ with $r_{g\min} = r_s$ is symmetrical with the conjugate of the stability circle with respect to the imaginary axis.

(c) The $G_{T\max} > G_T > 0$ circles always take place in the USWA. As the absolute stability case, all the compatible $(F, V_i, G_T)$ triplets take place in the intersection area between the PSR and USWA.

(d) In the conditional stability case, the maximum gain will be obtained on the arc of the conjugate stability circle remaining in the right half of the $Z_{\text{in}}$ plane. The maximum gain subject to the $V_i$ can be found by substituting $R_{cg} = R_{cs}$ in (27):

$$G_{T\max} = 2\frac{1 - |\rho_i|^2}{|z_{12}|^2}. \quad (28)$$

We have the Maximum Stable Gain (MSG)

$$\text{MSG} = 2\left|\frac{z_{21}}{z_{12}}\right|\eta, \quad \eta \triangleq \frac{2r_{11}r_{22} - r}{|z|}, \quad (29)$$

where $\eta$ is the stability factor with the values between zero and unity $(0 > \eta > 1)$.

## 3. SVRM Model of Microstrip Line

In this section, SVRM model of a microstrip line is presented. It is significant that SVRM model of microstrip line is as fast as analytical formulation and is highly accurate like 3D numerical simulations. The mathematical background and detailed theory of SVRM are explained in previous work [7]. In this study, epsilon SVR [16] is employed as SVM type and radial basis function is performed as kernel type. Input variables of model are line width ($W$), frequency ($f$), height ($h$), and relative permittivity ($\varepsilon_r$) of substrate material and corresponding output variables are characteristic impedance ($Z_0$) and effective relative permittivity ($\varepsilon_{\text{eff}}$). Because each machine has one output, there are two machines with the same inputs.

First of all, coarse model of microstrip line, which has a training data set acquired from quasi-TEM analytical formulations, is formed. Input and output variable values of training data set are given in Table 1. Furthermore, support vectors (SVs) and accuracy of coarse model are shown for different epsilon values in Table 2. The obtained support vectors are used to form training data set of fine model, such that these SVs are chosen as input variables of training data and output data is calculated with 3D electromagnetic simulator, as seen in Figure 4. Therefore, either training data number is reduced or duration of data set forming is shortened. The same SVR model and kernel type are used for fine model training. According to results of fine model, accuracy of characteristic impedance and effective permittivity are %99.4 and %99, respectively, and it is also 400 times faster than 3D EM simulator for 2.3 GHz CPU and 2 GB memory. As an example, Figure 5 shows characteristic impedance and effective relative permittivity variations subject to width of line for fine model ($\varepsilon_r = 2.94$, $h = 0.762$ mm). Consequently, expeditious and highly accurate model of microstrip line is ready to perform in optimization network.

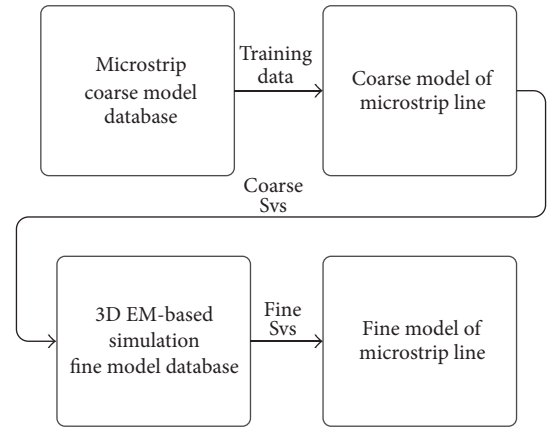


Figure 4: Cost effective 3D EM simulation-based Support Vector Microstrip Modeling.

Table 1: The range of values for SVRM training data set for coarse model.

| Parameters | Start value | Stop value | Interval |
|---|---|---|---|
| Width ($W$) | 0.1 mm | 4.6 mm | 0.5 mm |
| Height ($h$) | 0.1 mm | 2.2 mm | 0.7 mm |
| Permittivity ($\varepsilon_r$) | 2 | 10 | 2 |
| Frequency ($f$) | 2 GHz | 14 GHz | 3 GHz |
| Characteristic impedance ($Z_0$) | 3 ohms | 240 ohms | |
| Effective permittivity ($\varepsilon_{\text{eff}}$) | 1.5 | 9.7 | |

Table 2: SVRM parameters for coarse model.

| $\gamma$ | $C$ | Epsilon ($\epsilon$) | Number of "$Z_0$" SVs | Accuracy |
|---|---|---|---|---|
| 0.001 | 10000 | 0.05 | 583 | %99.4 |
| 0.001 | 10000 | 0.07 | 402 | %98.6 |
| 0.001 | 10000 | 1 | 279 | %97.9 |

## 4. Optimization

During the design optimization process, determining widths and lengths of microstrip lines in input and output matching network is objected, so that IMC and OMC provide source and load impedance which are obtained from performance

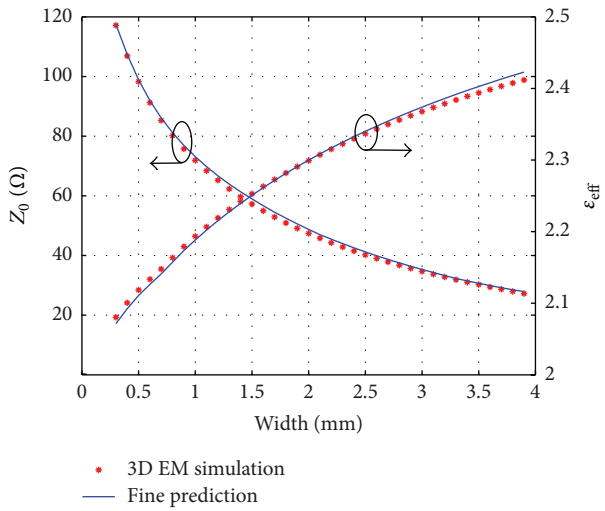


FIGURE 5: Comparative variations of characteristic impedance and effective dielectric constant versus width of the fine model and the 3D EM simulation on the substrate $\varepsilon_r = 2.94$, $h = 0.762$ mm at $f = 6$ GHz.

characterisation of employed transistor (NE3512S02) for minimum noise $F_{\text{req}}(\omega) = F_{\min}$, maximum gain $G_{T\text{req}}(\omega) = G_{T\max}$, and $V_{i\text{req}}(\omega) = 1.85$ input VSWR. For this purpose, gains of the input/output matching circuits ($G_T$) terminated by the $Z_{\text{Str}}{}^*(\omega)$ and the $Z_{L\text{tr}}{}^*(\omega)$ are maximized all over the requested operation band ($B_{\text{req}}$), as seen in Figure 1. In order to do that, the cost function is chosen as minimization of

$$\text{cost}\left(\vec{W}, \vec{\ell}\right) = \sum_{i=1}^{N} 1 - G_T\left(\vec{W}, \vec{\ell}, \omega_i\right), \tag{30}$$

where

$$G_T = \frac{4R_S R_L}{\left|AZ_L + B + Z_S\left(CZ_L + D\right)\right|^2}, \tag{31}$$
$$W_\ell \le W_i \le W_u, \quad \ell_\ell \le \ell_i \le \ell_u; \quad i = 1, \ldots, \Lambda,$$

where $A$, $B$, $C$, $D$, $Z_S$, and $Z_L$ parameters of matching circuit configurations are calculated using the cost effective SVRM model of the microstrip line given in Section 3 for chosen substrate $(\varepsilon_r, h)$. Also, $N$ is the number of the sampled frequencies within the bandwidth and is the element number of the matching circuit.

PSO algorithm is performed to minimize the cost function given by (30) with respect to the microstrip widths and lengths. PSO is a population based optimization method for an $N$-dimensional problem; the position and velocity of each particle can be specified by $M \times N$ matrices, where $M$ is the number of particles in the swarm.

Firstly, physical parameters, which are geometric limits of matching circuits, and convergence parameters, which are tolerance parameter ($\tau$) and maximum iteration number ($\kappa_{\max}$), of the algorithm are assigned. In the updating process, position, velocity, personal best, and global best matrices are launched randomly. For each iteration, cost function value is calculated for each particle and these values are used to determine each particle's personal best and global best value of the swarm. The algorithm ends when either the error or the iteration number reaches its assigned value. Comprehensive design optimization algorithm of the amplifier is depicted in Figure 6.

## 5. Design Example and Measurement

As a test vehicle of the presented methodology, the worked design example of typical wideband, low noise amplifiers using the $T$-types of microstrip matching circuits will be given. In design example, transistor NE3512S02 is used and Figure 7 gives the maximum gain variations constrained by the minimum noise figure, resulted from its performance characterisation at $V_{\text{DS}} = 2$ V and $I_{\text{DS}} = 20$ mA. From Figure 7, it is understood that there is no solution all over the operation band for every $V_i$ value and $V_i = 1.85$ is the most appropriate solution for both flat gain and mismatching as little as possible. In the design optimization process, the performance ($F_{\text{req}}(\omega) = F_{\min}(\omega)$, $V_{i\text{req}}(\omega) = 1.85$, and $G_{T\text{req}}(\omega) = G_{T\max}(\omega)$) triplet within the bandwidth of 3 GHz $\le f \le$ 8 GHz at the bias condition of $V_{\text{DS}} = 2$ V and $I_{\text{DS}} = 20$ mA is required as a design target and the real and reactive parts of the corresponding source and load terminations obtained by performance characterisation are trying to satisfy with matching circuits. As substrate material, RO 6002 is used $\{\varepsilon_r = 2.94, h = 0.762\text{ mm}, \tan\delta = 0.002, t = 0.035\text{ mm}\}$. In order to provide ultra-wideband DC bias of the transistor, ADCH-80A+ RF choke [17] is used in $T$-type of microstrip MCs, as seen in Figure 1. Moreover, in our PSO application, convergence happens between 150 and 300 iterations depending on the initialization values taking 2 minutes 37 seconds and 4 minutes 33 seconds, respectively, using 50 particles with 2.3 GHz CPU Processor, 2 GB RAM. After so many trials, best particles number is chosen as 50 for this application. Besides, PSO convergence parameters and maximum iteration number are taken as 0.005 and 300, respectively. Figure 8 shows convergence curve of cost function, where the convergence typically occurs within 200 numbers of iterations. After optimization process the designed amplifier is fabricated and measured. Picture of the manufactured ultra-wideband LNA is given in Figure 9 and the optimum values for the $T$-types of microstrip widths and lengths $\{\vec{W}, \vec{\ell}\}$ are found in Table 3. Furthermore the performances of the synthesized amplifier are compared using a microwave system circuit simulator and verified to agree with each other. Thus the targeted, synthesized, simulated, and measured performance ingredients gain, $V_i$, $V_{\text{out}}$, and noise with respect to the frequency are given for the amplifiers with the $T$-types of microstrip matching circuits in Figures 10, 11, 12, and 13, respectively.

## 6. Conclusions

In this work, the highly nonlinear design optimization problem of the linear regime microwave amplifiers is solved by a systematic and efficient methodology in which each

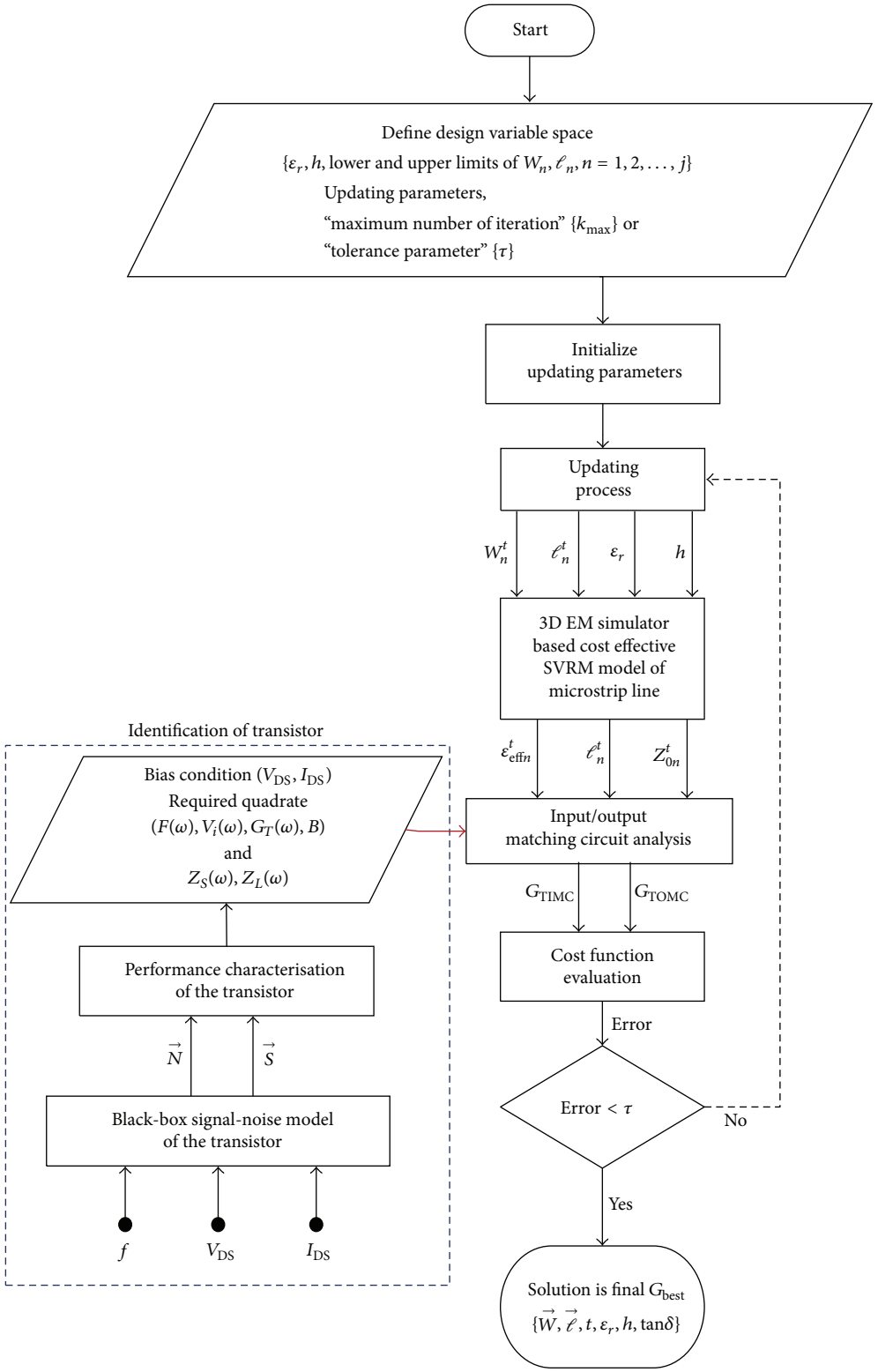


Figure 6: Block diagram of the performance characterisation-based design optimization of the matching circuits with the cost effective 3D EM-based Support Vector Microstrip Model.

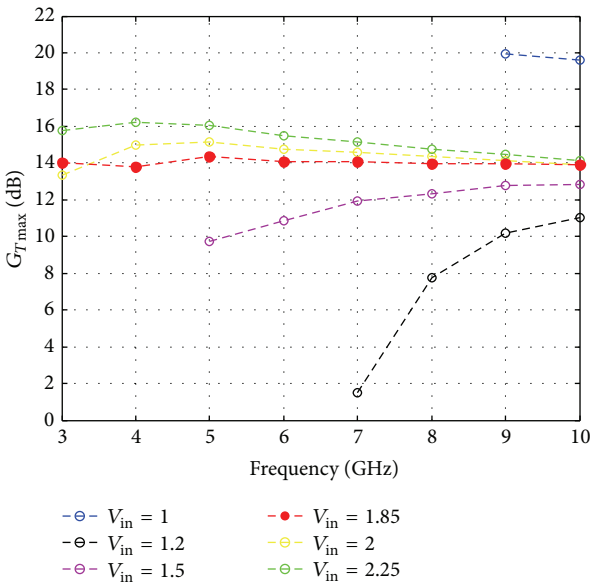


Figure 7: Maximum transducer gain for different input VSWR ($V_{DS}$ = 2 V, $I_{DS}$ = 20 mA, and $F_{req} = F_{min}$ dB).

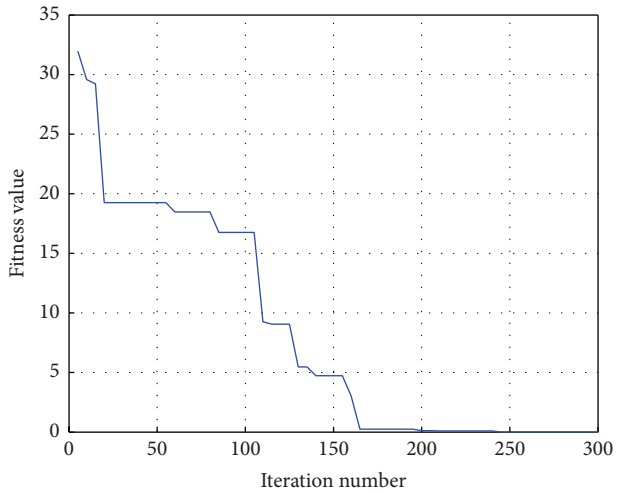


Figure 8: Cost function convergence curve.

Table 3: Solution space for the (T-T) IMC and OMC elements.

| $W_1$ (mm) | $W_2$ (mm) | $W_3$ (mm) | $W_4$ (mm) | $W_5$ (mm) | $W_6$ (mm) |
|---|---|---|---|---|---|
| 2,4 | 0,25 | 0,25 | 0,75 | 0,25 | 3 |
| $\ell_1$ (mm) | $\ell_2$ (mm) | $\ell_3$ (mm) | $\ell_4$ (mm) | $\ell_5$ (mm) | $\ell_6$ (mm) |
| 4,25 | 14,5 | 2,5 | 13 | 6,5 | 15,75 |

constituent of the optimization procedure is defined on the rigorous mathematical bases. First of all, identification of transistor is based upon the potential performance of the employed transistor in the form of interrelations among the operation parameters ($f, V_{DS}, I_{DS}$) and performance measure functions, gain, input VSWR, and noise, built by using the linear circuit and noise theories. Thus, this will enable the designer to choose the most proper compatible {noise

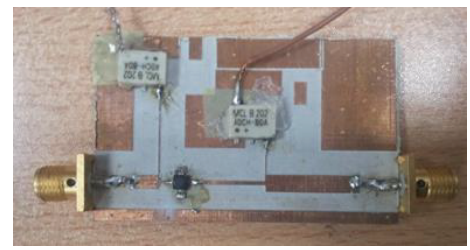

Figure 9: Fabricated UWB low noise amplifier.

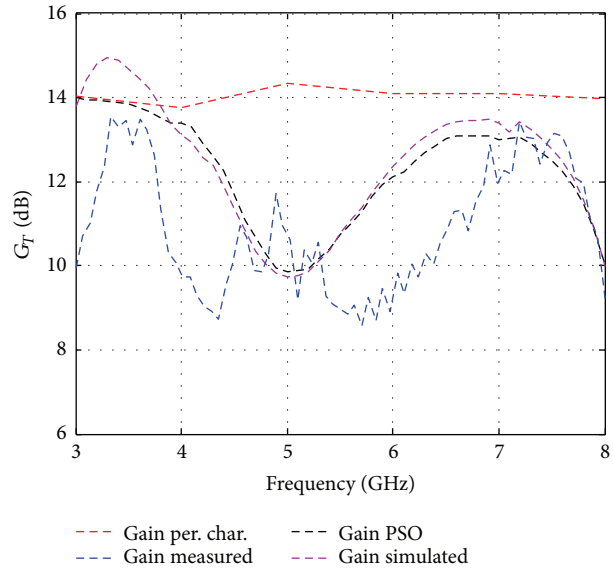


Figure 10: Comparative results for transducer gain of designed amplifier.

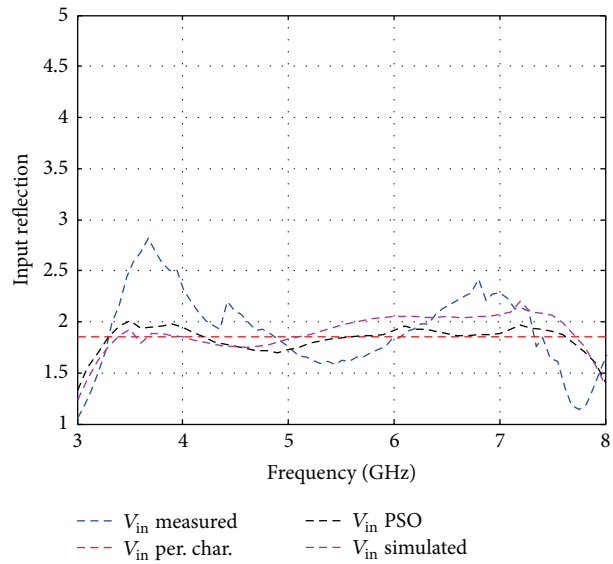


Figure 11: Comparative results for input VSWR of designed amplifier.

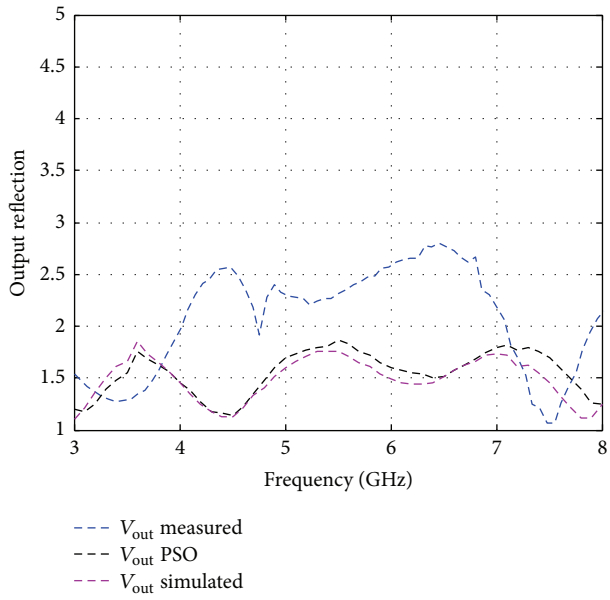


Figure 12: Comparative results for output VSWR of designed amplifier.

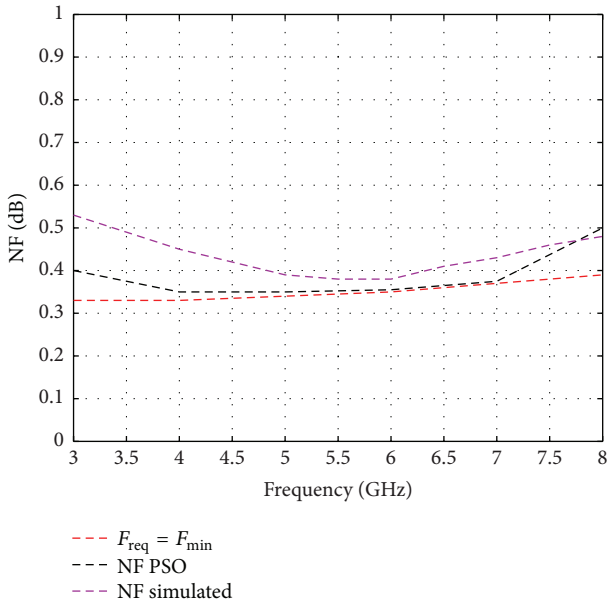


Figure 13: Comparative results for noise figure of designed amplifier.

$F(\omega) \geq F_{\min}(\omega)$, input VSWR $V_{in}(\omega) \geq 1$, gain $G_{T\min}(\omega) > G_T(\omega) \geq G_{T\max}(\omega)$, bandwidth $B\}$ quadrate as being aware of its advantages and disadvantages. The necessary source $Z_S(\omega)$ and load $Z_L(\omega)$ terminations will also be provided so that the multiobjective optimization is reduced into the two separate single objective scalar optimization processes within a design variable space subject to the technological limits. Another significant contribution of this work is to provide a fast, accurate, and cost effective model employing novel soft technology facilities in which the characteristic impedance $Z_0$ and the dielectric constant $\varepsilon_{\text{eff}}$ of the equivalent transmission line are expressed as the continuous functions to be used in the updating process. In this work, the 3D EM-based SVRM analysis model of the microstrip line has been provided to be used in the updating process. In the modelling process, the substantial reduction (by up to %60) is obtained utilizing sparseness of the standard SVRM in the number of expensive fine discretization training data with the negligible loss in the predictive accuracy in conjunction with the quasi-TEM microstrip synthesis formulae as the coarse data generator that allow identifying the regions of the design space requiring denser sampling. Besides, any convenient algorithm using either gradient or no gradient can be employed for the updating processes; in our case PSO is used for the accuracy and fast convergence.

Finally as the worked example, this design methodology is applied to the design of typical wideband low noise amplifiers of the transistor NE3512S02 on the dielectric substrate $\{\varepsilon_r = 2.94, h = 0.762\,\text{mm}, \tan\delta = 0.002, \text{and } t = 0.035\,\text{mm}\}$ within 3 GHz and 8 GHz satisfying $\{F_{\min}(f), V_{\text{in}} = 1.85, G_{T\max}(f)\}$ triplet using $T$-type of microstrip matching circuits. After that, the designed amplifier is manufactured and measured. Both simulated and measured results validate the predicted design with good agreement. It is concluded that this method, which is highly accurate as 3D EM simulator and fast as analytical solution, can also be applied as a robust method for the design and analysis of any microstrip amplifier synthesis.

## Conflict of Interests

The authors declare that there is no conflict of interests regarding the publication of this paper.

## References

[1] H. Fukui, "Available power gain, noise figure, and noise measure of two-ports and their graphical representations," *IEEE Transactions on Circuit Theory*, vol. 13, no. 2, pp. 137–142, 1966.

[2] H. Fukui, "Design of microwave GaAs MESFET's for broadband low-noise amplifiers," *IEEE Trans Microwave Theory Tech*, vol. 27, no. 7, pp. 643–650, 1979.

[3] A. Dobrowolski, *Introduction to Computer Methods for Microwave Circuit Analysis and Design*, Artech House, Norwood, Mass, USA, 1991.

[4] G. Gonzales, *Microwave Transistor Amplifiers*, Prentice-Hall, London, UK, 1996.

[5] Z. Marinković, O. Pronić-Rančić, and V. Marković, "Small-signal and noise modeling of class of HEMTs using knowledge-based artificial neural networks," *International Journal of RF and Microwave Computer-Aided Engineering*, vol. 23, no. 1, pp. 34–39, 2013.

[6] Q.-J. Zhang, K. C. Gupta, and V. K. Devabhaktuni, "Artificial neural networks for RF and microwave design—from theory to practice," *IEEE Transactions on Microwave Theory and Techniques*, vol. 51, no. 4, pp. 1339–1350, 2003.

[7] F. Güneş, N. T. Tokan, and F. Gürgen, "A knowledge-based support vector synthesis of the transmission lines for use in microwave integrated circuits," *Expert Systems with Applications*, vol. 37, no. 4, pp. 3302–3309, 2010.

[8] F. Güneş, M. Güneş, and M. Fidan, "Performance characterisation of a microwave transistor," *IEE Proceedings: Circuits, Devices and Systems*, vol. 141, no. 5, pp. 337–344, 1994.

[9] F. Günes and B. A. Çetiner, "A novel Smith chart formulation of performance characterization for a microwave transistor," *IEE Proceedings—Circuits, Devices and Systems*, vol. 145, pp. 419–428, 1998.

[10] N. Telzhensky and Y. Leviatan, "Novel method of UWB antenna optimization for specified input signal forms by means of genetic algorithm," *IEEE Transactions on Antennas and Propagation*, vol. 54, no. 8, pp. 2216–2225, 2006.

[11] S. Chamaani, M. S. Abrishamian, and S. A. Mirtaheri, "Time-domain design of UWB vivaldi antenna array using multiobjective particle swarm optimization," *IEEE Antennas and Wireless Propagation Letters*, vol. 9, pp. 666–669, 2010.

[12] D. Swanson and G. Macchiarella, "Microwave filter design by synthesis and optimization," *IEEE Microwave Magazine*, vol. 8, no. 2, pp. 55–69, 2007.

[13] R. Menozzi, A. Piazzi, and F. Contini, "Small signal modeling for microwave FET linear circuits based on a genetic algorithm," *IEEE Transactions on Circuits and Systems I: Fundamental Theory and Applications*, vol. 43, no. 10, pp. 839–847, 1996.

[14] R. Eberhart and J. Kenedy, "A new optimizer using particle swarm theory," in *Proceedings of the 6th International Symposium on Micro Machine and Human Science (MHS '95)*, pp. 39–43, Cape Cod, Mass, USA, 1995.

[15] R. Eberhart and J. Kennedy, "Particle swarm optimization," in *Proceedings of the IEEE International Conference on Neural Networks*, pp. 1114–1121, Piscataway, NJ, USA, December 1995.

[16] V. N. Vapnik, *The Nature of Statistical Learning Theory*, Springer, New York, NY, USA, 1995.

[17] 2015, http://194.75.38.69/pdfs/ADCH-80A.pdf.